Evaluation of the chondral modeling theory using fe-simulation and numeric shape optimization

Jeffrey H. Plochocki,[1] Carol V. Ward[2] and Douglas E. Smith[3]

[1]*Department of Anatomy, Midwestern University, Glendale, AZ, USA*
[2]*Department of Pathology and Anatomical Science, University of Missouri at Columbia, Columbia, MO, USA*
[3]*Department of Mechanical and Aerospace Engineering, University of Missouri at Columbia, Columbia, MO, USA*

Abstract

The chondral modeling theory proposes that hydrostatic pressure within articular cartilage regulates joint size, shape, and congruence through regional variations in rates of tissue proliferation. The purpose of this study is to develop a computational model using a nonlinear two-dimensional finite element analysis in conjunction with numeric shape optimization to evaluate the chondral modeling theory. The model employed in this analysis is generated from an MR image of the medial portion of the tibiofemoral joint in a subadult male. Stress-regulated morphological changes are simulated until skeletal maturity and evaluated against the chondral modeling theory. The computed results are found to support the chondral modeling theory. The shape-optimized model exhibits increased joint congruence, broader stress distributions in articular cartilage, and a relative decrease in joint diameter. The results for the computational model correspond well with experimental data and provide valuable insights into the mechanical determinants of joint growth. The model also provides a crucial first step toward developing a comprehensive model that can be employed to test the influence of mechanical variables on joint conformation.

Key words chondral modeling; joint growth; knee; finite element method; numeric shape optimization.

Introduction

The maintenance of joint congruence during mammalian skeletal morphogenesis is imperative for retaining joint mobility and stability during growth. Joint congruence also prevents the accumulation of high contact stresses by distributing loads more broadly across articular surfaces (Stone & Yu, 1997). Even a minor incongruence on the order of 0.3% can significantly increase concentrated contact stresses associated with harmful local cartilage strains (Stone & Yu, 1997; von Eisenhart-Rothe et al. 1997) that may lead to degenerative joint disease in humans (Mow et al. 1989; Brandt et al. 1991; Kippel & Dieppe, 1994). Joint conformation must therefore follow a trajectory that maintains a normal kinematic pathway as the magnitudes and orientations of joint loads change throughout postnatal ontogeny.

Functional adaptation of joints to the mechanical environment during skeletal morphogenesis is hypothesized to occur through the transduction of mechanical energy in articular cartilage (Frost, 1999; Hamrick, 1999; Heegaard et al. 1999; Carter & Beaupré, 2001). Although the specific intracellular pathways that transduce mechanical signals are unclear, chondrocyte metabolism and gene expression are influenced by the mechanical deformation of cartilage from loading (Urban, 1994; Smith et al. 1996; Guilak et al. 1997; Elder et al. 2001; Wagner et al. 2008). Of particular importance is the distribution of hydrostatic pressure in articular cartilage following loading. *In vitro* experiments show that chondrocytes exposed to 1–10 MPa of intermittent hydrostatic pressure exhibit increases in cellular metabolism, whereas loads above 10 MPa slow chondrocyte differentiation (Takahashi et al. 1995; Smith et al. 2000; Wong et al. 2003). Thus, rates of cartilage tissue proliferation are regulated by levels of hydrostatic pressure. Because chondrocyte metabolism directly affects subchondral bone growth during endochondral ossification, the hydrostatic stress state of articular cartilage also regulates the growth of bony articular surfaces.

The chondral modeling theory, first proposed by Frost (1999) and later modified by Hamrick (1999), postulates that hydrostatic pressure in articular cartilage affects joint conformation in a manner than maintains joint congruence throughout development while minimizing the risk of tissue damage. Based on experimental data from cartilage explants, the chondral modeling theory predicts that low to moderate hydrostatic pressure (1–10 MPA) will maintain or accelerate growth, whereas regions of high hydrostatic

Correspondence

Jeffrey H. Plochocki, Ph.D., Arizona College of Osteopathic Medicine, Midwestern University, 19555 N 59thAve, Glendale, AZ 85308 USA. E: jploch@midwestern.edu

Fig. 1 Two-dimensional finite element model of the human tibiofemoral joint medial to the midsagittal plane. Anterior side is to the left. The thicker lines separate the femoral articular cartilage, the meniscus, and tibial articular cartilage.
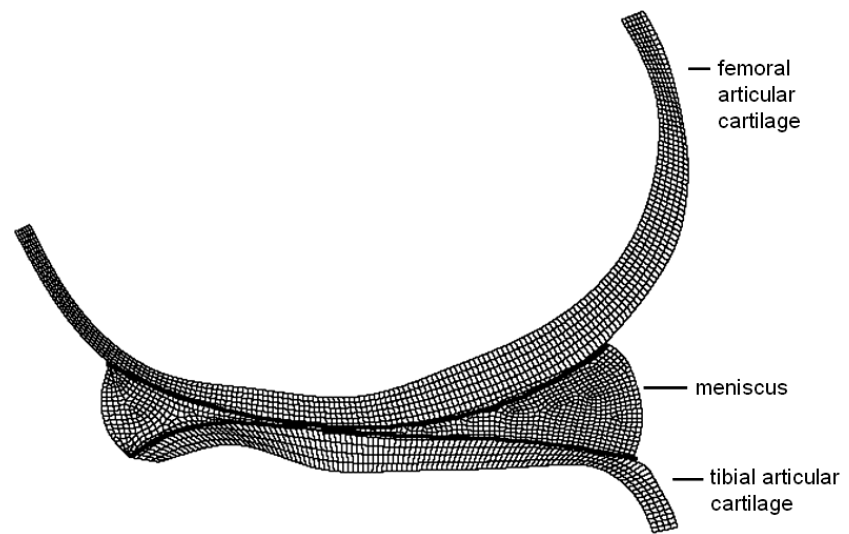
pressure (> 10 MPA) will experience slowed or arrested growth (Hamrick, 1999). Such growth would produce an articular surface topography that maximizes hydrostatic pressure in articular cartilage because tissue proliferation would continue in areas of low and moderate hydrostatic pressure until a high pressure state was achieved and growth would stop. The maximization of hydrostatic pressure would be best achieved through total joint congruence (Frost, 1999). Growth that maximizes the distribution of hydrostatic pressure would also minimize shear stress, which has an inhibitory effect on chondrocyte metabolism that contributes to tissue degeneration (Wong & Carter, 2003, Smith et al. 2004).

Modifications in joint morphology have been identified in experimental studies using animal exercise models and in clinical observations (Murray et al. 2001; Frost, 1972, 1979; Steinberg & Trueta, 1981; Radin et al. 1982; Bouvier & Zimny, 1987; Plochocki et al. 2006). However, the stress state of articular cartilage is difficult to measure *in vivo*, making it troublesome to correlate articular stress directly with changes in joint morphology during growth. The objective of the current study was to develop a simple two-dimensional, nonlinear finite element model of the human tibiofemoral joint which could be used to test basic hypotheses implicit in the chondral modeling theory. A further aim of the study is to provide an initial step towards developing a three-dimensional finite element model of the knee that could be used to study the complex variables associated with the mechanical influences on joint conformation. Because the motion, loading, and tissue material properties of the human knee joint are simplified in our model, we address only broad predictions made by the chondral modeling theory. We test the following hypotheses: (1) articular surface modifications from chondral modeling will expand the distribution of loads across articular cartilage to reduce high strain concentrations

that damage tissue, (2) the curvature of the articular surfaces will adapt to enlarge the adjacent bony joint contact area during periods when peak transarticular loads occur, (3) adjacent articular surfaces will remain congruent throughout growth, and (4) a relative decrease in the size of the articular surfaces will occur.

Material and methods

Finite element model

A magnetic resonance (MR) image of the medial tibiofemoral joint in full extension from a 12-year-old male human was digitized using a flatbed scanner (Laor et al. 2002). Coordinate continuous data depicting the boundaries of the femur, tibia, articular cartilages, and medial meniscus were recorded using the software TPSDIG version 1.23 (Rohlf, 1998). The threshold levels of the image were manipulated to obtain the clearest boundary between tissues to minimize error. Digitization of joint tissue from MR images may result in minor geometric variability, but are generally reliable (Guoan et al. 2001). Coordinate data were then imported into the finite element program HYPERMESH (Altair Engineering, Inc., 2000) and used to generate a two-dimensional finite element model of the medial tibiofemoral joint comprising plane stress elements (Fig. 1). The finite element mesh was then exported for input into ABAQUS 6.3 (Hibbitt et al. 2002) general purpose finite element program, which was used to perform all joint stress analysis simulations (e.g. see Huebner et al. 2001).

The material properties for all tissues in the model were assumed to be linear elastic. Articular cartilage was modeled with an elastic modulus of 6.0 MPa to be consistent with experimental data and other linear elastic investigations of cartilage mechanobiology (Lyyra et al. 1995; Beaupré et al. 2000; Carter & Wong, 2003; Saarakkala et al. 2004). Because the high water content of articular cartilage makes the tissue nearly incompressible (Armstrong et al. 1984), cartilage was modeled with a Poisson's ratio of 0.49. The medial meniscus was modeled with a modulus of 20 MPa and Poisson's ratio of 0.20 (Fithian et al. 1989; Tissakht & Ahmed, 1995). A spring with a rate of 9.21 N mm^{-1} was included that linked the
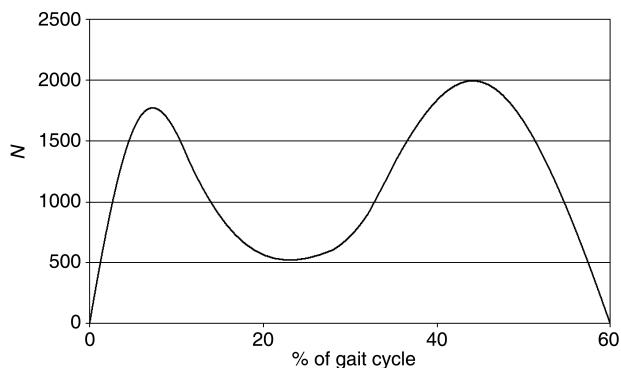
Fig. 2 Amplitude curve of tibiofemoral force used in the model during the simulation of stance phase loading of the gait cycle.

Fig. 3 Optimization routine.

anterior and posterior portions of the medial meniscus to allow the tissue to respond as a single biological structure. The femur and tibia were modeled as rigid surfaces to increase computational efficiency. When contact stresses of soft tissue on bone are being considered in finite element models of synovial joints, it is common to model the bone at the joint surface as rigid (Ferguson et al. 2000; Genda et al. 2001; Li et al. 2001; Godest et al. 2002; Donahue et al. 2003). Treating bone as a rigid surface has been shown to have a negligible effect on the stresses in joint soft tissue (Dalstra et al. 1995; Donahue et al. 2002).

Flexion of the tibia relative to the femur was simulated using displacements of the tibia in the sagittal plane. Joint motion in the finite element model was consistent with flexion and anterior–posterior translational motion described in the literature (Wretenberg et al. 2002). A follower load, defined to rotate as nodes in the model rotate, was applied to the tibia to keep the joint force parallel to the tibia shaft throughout joint flexion. The magnitude of the load was modified during flexion using an amplitude curve (Fig. 2) that provided a maximum load of 2000 N, which is typical during normal gait loading of the medial tibiofemoral joint (Thambyah et al. 2005). The load was fluctuated over a 0.5-s stance phase of gait in a manner characteristic of tibiofemoral contact forces (Hurwitz et al. 1998; Shelburne et al. 2006). Contact between articular cartilage of the tibia and femur and the meniscus were modeled as frictionless finite sliding of deformable bodies against deformable bodies. The articular cartilages were bound to the bony surfaces of the tibia and femur using tied contact that restricted motion between the cartilage and bone. No penetration was allowed at any of the nodes.

Optimization routine

Stress-regulated shape-change of the tibiofemoral joint as predicted by the chondral modeling theory was simulated using numeric optimization in conjunction with a finite element analysis. A joint shape prediction routine was created to integrate these two procedures as illustrated in Fig. 3. The routine begins with a definition of the joint shape that was used to construct the finite element mesh. The elements and nodal locations were then imported for finite element analysis using ABAQUS (Hibbitt et al. 2002). Stresses computed in ABAQUS served as input to the numeric optimization software VISUALDOC (Vanderplaat, 2002a), which performed a gradient-based optimization procedure. Changes in the design parameters as defined by VISUALDOC were then written
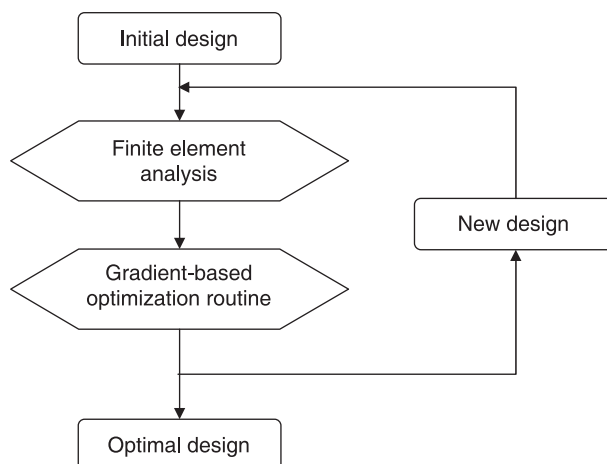
to a Hypermesh command file, which reconfigured and remeshed the finite element model. The process was repeated until the optimal design was achieved. The entire process was automated by a computer script created with the program VISUALSCRIPT (Vanderplaat, 2002b). The script relayed the design parameters and the objective function values between ABAQUS, VISUALDOC, and HYPERMESH.

Optimization design parameters and objectives

The design parameters in the optimization problem defined as distances that control nodes on the femoral and tibial articular surfaces were moved to produce changes in articular surface shape (Fig. 4). Twenty control nodes were employed to produce articular shape change – 10 on the femoral articular surface and 10 on the tibial articular surface. To capture the topography of the articular surface, control nodes were placed roughly equidistant from each other at points where changes in the contour of the articular surface were apparent. Side constraints were placed on the design parameters to limit modifications in articular shape and therefore give more realistic results for normal bone growth (i.e. simulate bone formation from columns of chondrocytes in articular cartilage). These constraints prevented the control nodes from moving more than 5 mm in a direction normal to the existing articular surface. The sensitivity of the model to alterations in the placement of the control nodes was evaluated by repositioning the control nodes along the geometry representing the articular surfaces and re-executing the optimization procedure. Overlays of the optimized geometries were congruent in shape, suggesting the model is robust to minor alterations in control node placement along the geometric surfaces.

Changes in the design parameters were used to alter the shape of the finite element model and produce a new joint design. The articular surfaces were redefined by fitting a cubic spline through the repositioned control nodes. The joint soft tissues in the model were then remeshed to conform to the new bone surface shape. Cartilage and meniscus thicknesses were held constant throughout the analysis. Although articular cartilage thickness declines during development, the rate and distribution of this change is not known and could not be modeled accurately.
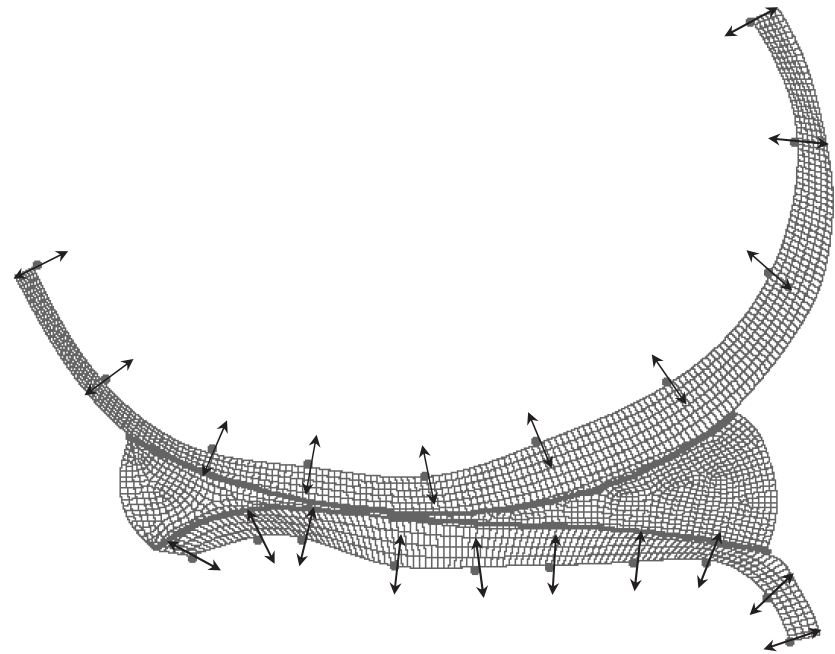
Fig. 4 Allowable movement of the control nodes set up in the finite element model. The arrows indicate the direction of allowable movement. The control nodes were moved along vectors adjacent to the surface normal in the shape optimization analysis. Following each optimization iteration, the finite element model was reconfigured such that nodes on the articular surfaces were made coincident with the adjusted control nodes. Anterior side is to the left.

The objective of the optimization procedure was to maximize the hydrostatic pressure in the articular cartilage by modifying the shape of the femoral and tibial articular surfaces. Chondral modeling theory predicts that articular surface growth occurs differentially across the joint surface, slowing or stopping in areas of high hydrostatic pressure. Such growth would produce an articular surface topography that maximizes hydrostatic pressure in articular cartilage because growth would only continue in areas of low and moderate hydrostatic pressure and not in areas of high hydrostatic pressure.

The mathematical form of the optimization may be stated as

Find $\quad\quad \mathbf{X}$

To maximize $\quad f(\mathbf{x}) = \dfrac{1}{2n} \sum_{i=1}^{n} \left\{ \max[p_i^F(\mathbf{x})] + \max[p_i^T(\mathbf{x})] \right\}$

Subject to $\quad\quad x^L \leq x_j \leq x^U, \quad j = 1, 2, N$

where $\mathbf{x} = \{x_1, x_2, \dots x_N\}$ is a vector of the N design variables that define the geometry of the articular surfaces. In this study, each of the $N = 20$ design variables defined the location of a control node in the finite element model shown in Fig. 4. Ten of the design variables define the femoral surface, and the remaining 10 define the tibial surface. The design variables are limited by the side constraints where $x^L = -5$ mm and $x^U = 5$ mm. In the optimization problem given above, $f(\mathbf{x})$ is the objective function to be maximized which provides a scalar measure of the maximum hydrostatic pressure in the articular cartilage. The maximum hydrostatic pressure in the femoral cartilage $\max[p_i^F]$ and the tibial cartilage $\max[p_i^T]$ are averaged over the $n = 9$ position increments analyzed in our finite element analyses during joint flexion. Note that the objective function may only be evaluated once a complete finite element solution which computes the $\max[p_i^F]$ and $\max[p_i^F]$ is complete. All pressures are evaluated at the element centroids in our simulations.

In the current study, the optimization problem given above is solved with the Broyden-Fletcher-Goldfarb-Shanno (BFGS) unconstrained optimization algorithm (see Arora, 1989; Smith, 1997) implemented in the general purposed numerical optimization software program VisualDOC (Vanderplaats, 2002a). This algorithm has been used extensively, and has proven to be stable and reliable in many engineering applications (Arora, 1989; Gill et al. 1981; Ghosh et al. 2000). In each iteration of the optimization task, a search direction was computed based on the gradient of the objective function $f(\mathbf{x})$. These gradients (or design derivatives) were computed by VisualDOC using the forward finite difference method (e.g. see Huebner, et al. 2001). A line search is then performed along the search direction where a single variable quadratic approximation is maximized to determine the step size that is used to update the design variable vector $\mathbf{x}$. Convergence of the optimization procedure is determined when the absolute change in the $f(\mathbf{x})$ between optimization iterations is less than 0.0001.

The numerical optimization procedure provides a means to simulate shape changes that are predicted to occur by the chondral modeling theory. Although no growth is occurring in the model, the shape changes are hypothesized to reflect stress-regulated growth of the articular surface. The span of growth period in this simulation is from age 12 to skeletal maturity as the initial finite element geometry is generated from a 12-year-old male and tibio-femoral growth ceases at skeletal maturity. It should be noted that this model does not attempt to predict changes in absolute joint size during growth, but instead only defines shape modifications that better accommodate the stress state in the cartilage.
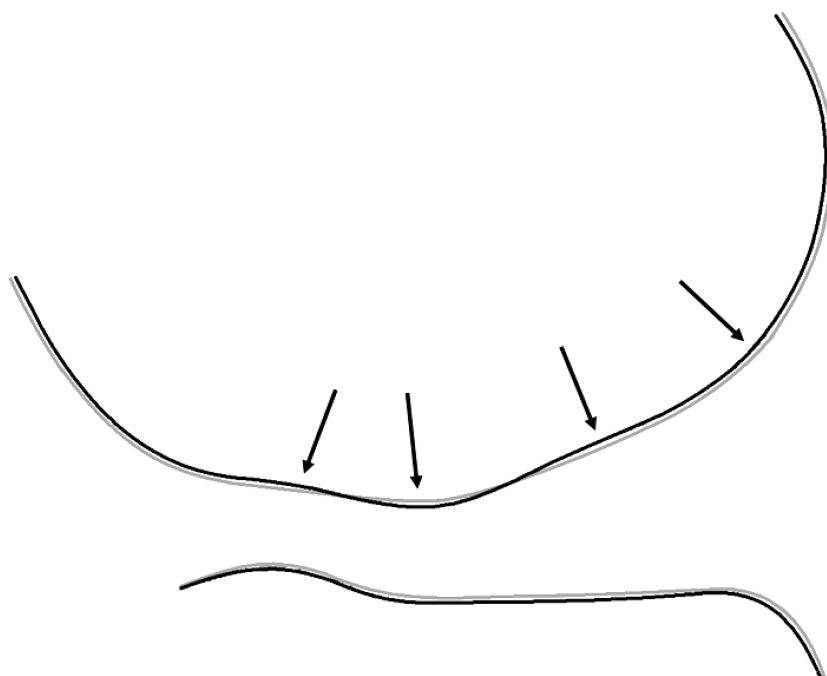
Results

The numeric shape optimization was completed successfully with five design iterations. The iteration history plot of the objective function $f(\mathbf{x})$ is shown in Fig. 5. Hydrostatic pressure in the articular cartilage increased with each successive design iteration from $f(\mathbf{x}) = 1.34$ MPa to $f(\mathbf{x}) = 1.76$ MPa for the optimal shape. Control nodes moved an average of 0.6 mm (range: −1.7 to 1.0 mm) from their position in the original model.
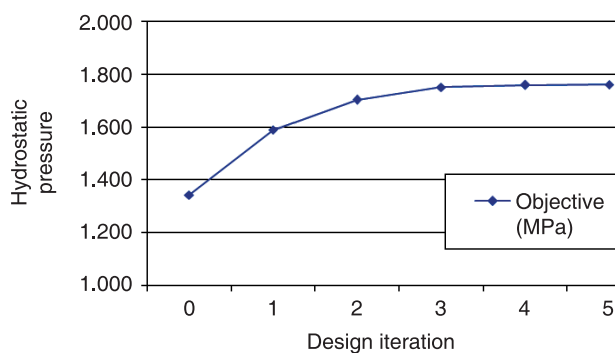
Fig. 5 Optimization objective improvement. The average maximum levels of hydrostatic pressure (MPa) in the femoral and tibial articular cartilage throughout the optimization process.

Articular surface outlines of the initial model and the optimal model are shown in Fig. 6. Overall, the shape-changes can be characterized as increasing articular surface congruence. The largest change is exhibited in the anterior-distal portion of the femoral joint surface. Here, the curvature becomes modified to reflect that of the tibia. Conversely, the posterior-distal portion of the femoral articular surface becomes slightly flattened, increasing contact area during flexion from an extended position. The curvature of the tibia becomes modified only slightly. The anterior convexity of the tibia exhibits a small reduction from the initial configuration. The posterior tibial articular surface shows virtually no change in shape. Both the femoral and tibial articular surfaces show a relative decrease in size from the initial model.

Finite element analyses of the tibiofemoral models show that the overall hydrostatic pressure state is improved by the optimization procedure. Contour plots of hydrostatic pressure at three degrees of joint flexion for the initial and final optimal model are displayed in Fig. 7. The final optimal models show more uniform distributions of the stresses throughout the articular cartilages, with a 31.3% increase in the average maximum hydrostatic pressure.

Discussion

The goal of the current study was to verify the chondral modeling theory by computing regional variations in articular morphology in response to hydrostatic pressure. The results presented here support the chondral modeling theory and provide a logical first step in developing a more complex computational model to aid in the under-standing of mechanical influences on joint conformation. Our analysis has several limitations that should be considered accordingly. The model simulated growth-related shape changes on a single joint configuration based on habitual loading during stance phase of gait, thus the broad applicability of our results remains unclear. Further, the simplifications made in the finite element analysis, particularly the assumptions of 2D and the homogeneous mechanical properties of the materials in the model, may have some effect on the stress distributions in the joint tissue. Also, the in-plane resolution of the MR image was 0.5 mm and the average nodal movement was 0.6 mm, thus nodal-movement shown by the simulations are partly within the imaging error caused by the image resolution.
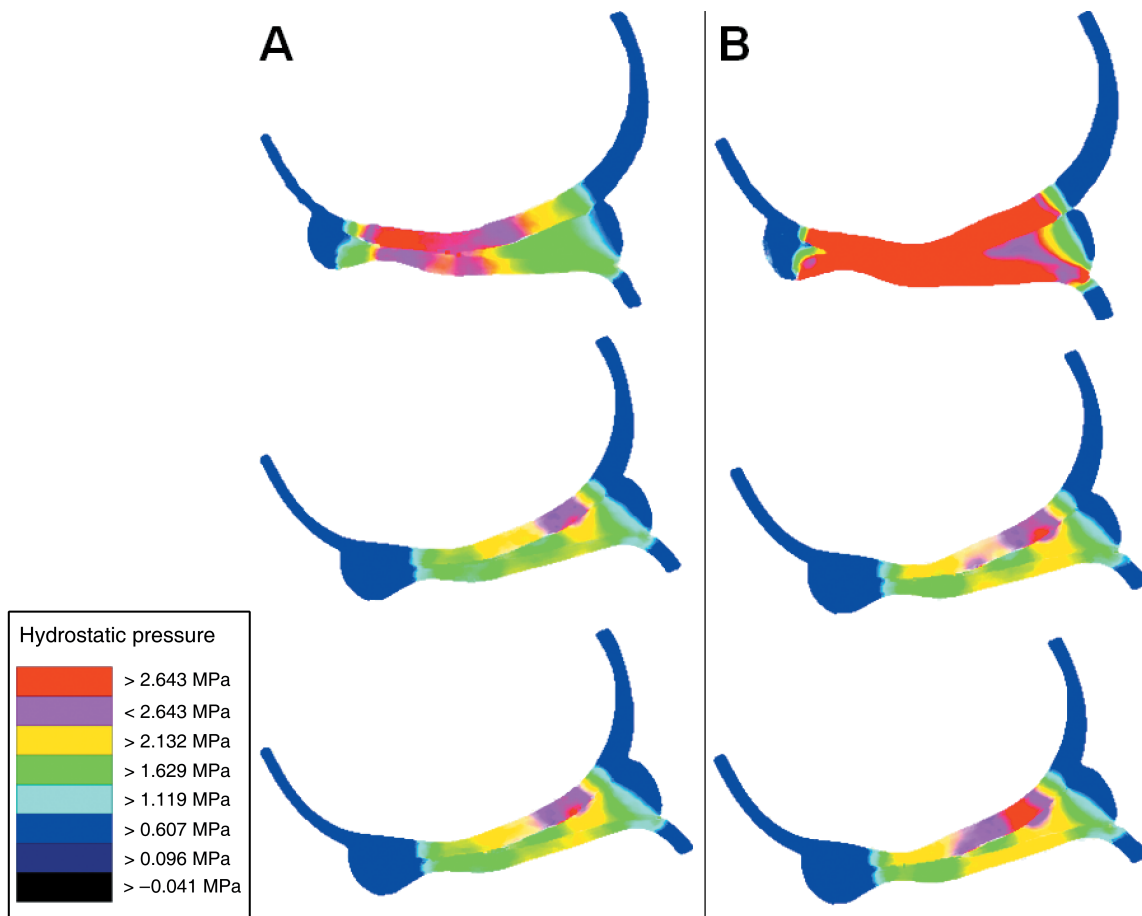

Fig. 6 Articular surface shape outlines of the initial model (light line) and optimal model (dark line). Anterior side is to the left. The arrows indicate areas of morphological change between the initial design and the final model.

Fig. 7 Contour plots of hydrostatic compressive stress in the initial (A) and optimal (B) models simulating joint flexion between initial contact (top) and terminal stance (bottom) during gait. The legend applies to both A and B.

However, modifications in articular form during skeletal morphogenesis subsequent to differential mechanical loading are well documented in experimental studies (Murray & Drachman, 1969; Steinberg & Trueta, 1981; Radin et al. 1982; Bouvier & Zimny, 1987; Eckstein et al. 2002; van de Lest et al. 2002; Plochocki et al. 2006), as are chondrocytic responses to hydrostatic pressure (Hamrick, 1996; Smith et al. 1996, 2000; Hutton et al. 2001; Sironen et al. 2002; Ikenoue et al. 2003; Toyoda et al. 2003). These findings are consistent with our results and the chondral modeling theory, which predicts specific modifications in joint form given specific magnitudes of hydrostatic pressure.

The accuracy of the optimization procedure was evaluated through comparisons of the optimized shape to three MR images of adult tibiofemoral joints (from Kaplan et al. 1999; Hauger et al. 2000; Helms, 2002). As our model attempts to provide only a broad analytical basis for clinical and experimental observations of chondral modeling, the evaluation is limited to qualitative comparisons of morphological similarities to adult specimens. Although

quantitative comparisons are ideal, qualitative comparisons are valuable for evaluating computational simulations that cannot be directly validated experimentally (Huiskes, 1997). Comparisons show that the articular profiles from the optimal model correspond well with those from the adult MR images (Fig. 8). The contours of the articular surfaces in the optimal design do not reflect irregular bony profiles, but profiles analogous to those of normal adults. As indicated by the three anterior arrows (arrows numbered 1, 2, and 3) in Fig. 8, an s-shaped curve becomes visible on the anterior-distal femoral surface that corresponds with the articular outline of the tibial joint surface, increasing articular congruence. In the optimal model, the anterior-distal curvature of the femur is modified to match that of the anterior tibia. The improved congruence resulting from the optimization process increased the contact areas between the tibia and femur during periods of full extension, thereby providing a structure that distributes stress over a larger portion of the articular surface. It is during periods of full extension in normal gait that the anterior-
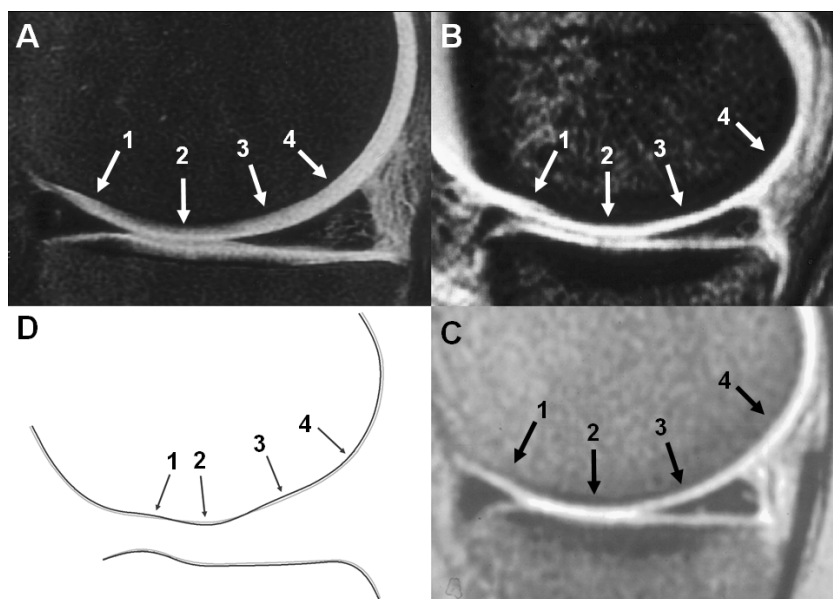
Fig. 8 Magnetic resonance images of three separate individual adult medial tibiofemoral joints from (A) Hauger et al. (2000), (B) Kaplan et al. (1999) and (C) Helms (2002) and (D) the articular surface outlines after completion of the optimization process. The articular surface outlines from the model (D) have been scaled to the size of the MR images (A–C). Anterior is to the left. The arrows point to shape-related features not present in the initial model but present in the optimal model. All of these features are present on the adult MR images. The arrows indicate areas of morphological change between the initial design and the final model.

distal portion of the femur is in contact with the tibia and contact pressures are greatest (Vaughan et al. 1997). In this regard, the anterior portion of the model is adapted to the peak hydrostatic compressive stresses that occur during initial contact (heel strike) in normal adult gait. Stresses become more widely distributed through an increased congruence during full extension (see top of Fig. 7).

In the optimal model, a slight posterior bulge indicated by arrow 4 in Fig. 8 also emerges on the posterior half of the distal femoral surface. The bulge divides the posterior portion of the femoral articular surface into two flatter sections that increase congruence during extension and flexion. During full extension, the angle and length of the distal portion of this curvature (anterior to the arrow) is such that it corresponds with the posterior portion of the medial meniscus and posterior tibial articular surface. Again, the femoral articular shape is adapted to increase congruence with the meniscus and tibia during full extension when contact stresses are greatest during initial contact. Further, the flattened area of the femoral articular surface maintains a more uniform stress distribution relative to the initial model in the ranges of flexion that occurs during normal gait (see Fig. 7).

The tibial articular surface in the optimal model exhibits only minor changes, but still corresponds with the adult MR images. The absence of large changes in the tibial articular surface is expected. Because the articular surface of the tibia is relatively flat and smooth in the initial model, stress gradients are more uniform across large portions of the joint surface (see Fig. 7). Under conditions where large loads per unit area are not present, as in the tibia in the optimal model, chondral modeling should not induce significant shape changes.

Contrary to the tibial articular surface, the femoral articular surface exhibited relatively larger shape changes due to more pronounced stress gradients in the femoral articular cartilage in the initial design model. The optimal model reduced high stress concentrations by distributing hydrostatic pressure across larger portions of the joint through alterations in femoral articular shape. The femoral articular surface, therefore, experienced greater relative changes in shape than the tibial articular surface. However, the optimization procedure was completed in only five design iterations. This suggests that the configuration of the initial model was nearly optimal for maximizing the hydrostatic stress state in the cartilage tissue of both the femur and tibia. Few design iterations were expected because the process of chondral modeling is continuous during development and it is unlikely that large deviations from such morphology would be present in the initial model.

Another effect of the tibiofemoral shape optimization was a decrease in size of the articular surface diameters relative to that of the initial configuration of the model (see Fig. 6). Relative joint size has been shown to decrease throughout ontogeny. For example, human joint diameters are larger in infants than in adults relative to body size (Williams, 1995, Fig. 6.12). Similar patterns have been observed in rat joint diameters (Hamrick, 1999), indicating joint stresses increase during skeletal maturation. The results presented here parallel this observation. The diameter across the femoral and tibial joint surfaces is smaller in the optimal model than in the initial model as predicted by the

chondral modeling theory. Joint size decreases, increasing hydrostatic pressure with age as the loads are transmitted through increasingly smaller surface areas. Diminishing joint diameter size also broadens the distribution of the stresses across the joint as seen in Fig. 7.

All of the changes observed between the initial and optimized model maximize hydrostatic pressure and expand its distribution. By maximizing hydrostatic pressure, harmful shear stresses are subsequently reduced in the tissue. Shear strain along collagen fibrils in cartilage is associated with the initiation of tissue degeneration (Wilson et al. 2005) and inhibits type II collagen and aggrecan synthesis by chondrocytes (Smith et al. 2004). Thus, tissue morphology in the optimized model decreases the risk of future tissue damage from the initial state.

In summary, the results of this study support predictions made by the chondral modeling theory. The chondral modeling theory predicts that articular growth occurs differentially across the joint surface such that peak pressures tend to become averaged across the articular surface, joint contact areas increase during periods of high transarticular loading, adjacent articular surfaces remain congruent throughout growth, and a relative decrease in joint size occurs to increase hydrostatic pressure within articular cartilage. We find that in the optimal model (1) joint surface congruence increased, retaining proper joint function and stability throughout joint flexion, (2) hydrostatic pressure increased and became more evenly distributed throughout the cartilage in the optimal model, a direct effect of increased congruence, (3) tibiofemoral contact area was enlarged throughout joint flexion, but particularly during full extension, also from increased joint congruence, and (4) the relative sizes of the tibial and femoral articular surfaces were decreased, increasing hydrostatic pressure in articular cartilage. Further development and refinement of the computational model is needed, however, to refine and expand our understanding of the relationship between the mechanical environment and limb joint growth.

Acknowledgements

References

Altair Engineering, Inc. (2000) *Hypermesh version 5.1*.

Armstrong CG, Lai WM, Mow VC (1984) An analysis of the unconfined compression of articular cartilage. *J Biomech Eng* **106**:165–73.

Arora J (1989) *Introduction to Optimum Design*. Boston: McGraw Hill.

Beaupré GS, Stevens SS, Carter DR (2000) Mechanobiology in the development, maintenance, and degeneration of articular cartilage. *J Rehab Res Dev* **37**, 145–151.

Bouvier M, Zimny ML (1987) Effects of mechanical loads on surface morphology of the condylar cartilage of the mandible in rats. *Acta Anat (Basel)* **129**, 293–300.

Brandt KD, Meyers SL, Burr DB, Albrecht M (1991) Osteoarthritic changes in canine articular cartilage, subchondral bone, and synovium fifty-four months after transection of the anterior cruciate ligament. *Arthritis Rheum* **34**, 1560–1570.

Carter DR, Beaupré GS (2001) *Skeletal Function and Form: Mechanobiology of Skeletal Development, Aging, and Regeneration*. Cambridge: Cambridge University Press.

Carter DR, Wong M (2003) Modelling cartilage mechanobiology. *Philos Trans R Soc Lond B Biol Sci* **1437**:1461–1471.

Dalstra M, Huiskes R, Vanerning L (1995) Development and validation of a 3-dimensional finite-element model of the pelvic bone. *J Biomech Eng* **111**, 272–278.

Donahue TLH, Hull ML, Rashid MM, Jacobs CR (2002) A finite element model of the human knee joint for the study of tibio-femoral contact. *J Biomech Eng* **124**, 273–280.

Donahue TLH, Hull ML, Rashid MM, Jacobs CR (2003) How the stiffness of meniscal attachments and meniscal material properties affect tibio-femoral contact pressure computed using a validated finite element model of the human knee joint. *J Biomech* **36**, 19–34.

Eckstein F, Faber S, Muhlbauer R, et al. (2002) Functional adaptation of joints to mechanical stimuli. *Osteoarthritis Cartilage* **10**, 44–50.

Elder SH, Goldstein SA, Kimura JH, Soslowsky LJ, Spengler DM (2001) Chondrocyte differentiation is modulated by frequency and duration of cyclic compressive loading. *Annnals Biomed Eng* **29**, 476–482.

Ferguson SJ, Bryant JT, Ganz R, Ito K (2000) The influence of the acetabular labrum on hip joint cartilage consolidation: a poroelastic finite element model. *J Biomech* **33**, 953–960.

Fithian DC, Schmidt MB, Ratcliffe A, Mow VC (1989) Human meniscus tensile properties: regional variation and biomechanical correlation. *Trans Orthop Res Soc* **35**, 205.

Frost HM (1972) *The Physiology of Cartilaginous, Fibrous, and Bony Tissue. Orthopedic Lectures Volume II*. Springfield, IL: Charles C Thomas.

Frost HM (1979) A chondral modeling theory. *Calc Tiss Int* **28**, 181–200.

Frost HM (1999) Joint anatomy, design and arthroses: Insights of the Utah paradigm. *Anat Rec* **255**, 162–174.

Genda E, Iwasaki N, Li G, MacWilliams BA, Barrance PJ, Chao EYS (2001) Normal hip joint contact pressure distribution in single-leg standing – effect of gender and anatomic parameters. *J Biomech* **34**, 895–905.

Ghosh DK, Garcelon JH, Balabanov VO, Venter G, Vanderplaats GN (2000) VisualDOC – a flexible design optimization software system. *Am Inst Aeronautics Astronautics* **4931**, 1–8.

Gill PE, Murray W, Wright MH (1981) *Practical Optimization*. London: Academic Press.

Godest AC, Beaugonin M, Huag E, Taylor M, Gregson PJ (2002) Simulation of a knee joint replacement during a gait cycle using explicit finite element analysis. *J Biomech* **35**, 267–275.

Guilak F, Sah RL, Setton LA (1997) Physical regulation of cartilage metabolism. In *Basic Orthopaedic Biomechanics* (eds Mow VW, Hayes WC), pp. 179–207. Philadelphia: Lippincott-Raven.

Guoan LI, Lopez O, Rubash H (2001) Variability of a three-dimensional finite element model constructed using magnetic resonance images of a knee for joint contact stress analysis. *J Biomech Eng* **123**, 341–346.

Hamrick MW (1996) Articular size and curvature as determinants of carpal joint mobility and stability in strepsirhine primates. *J Morphol* **230**, 113–127.

Hamrick MW (1999) A chondral modeling theory revisited. *J Theor Biol* **201**, 201–208.

Hauger O, Frank LR, Boutin RD, et al. (2000) Characterization of the 'red zone' of knee meniscus: MR imaging and histologic correlation. *Radiol* **217**, 193–200.

Heegaard JH, Beaupre GS, Carter DR (1999) Mechanically modulated cartilage growth may regulate joint surface morphogenesis. *J Orthop Res* **17**, 509–517.

Helms CA (2002) The meniscus: recent advances in MR imaging of the knee. *Am J Roentgenol* **179**, 1115–1122.

Hibbitt, Karlsson, and Sorensen, Incorporated (2002) *ABAQUS version 6.3*.

Huebner KH, Dewhirst DL, Smith DE, Byrom TG (2001) *The Finite Element Method for Engineers*, 4th edn. New York: John Wiley and Sons.

Huiskes R (1997) Validation of adaptive bone-remodeling simulation models. In *Bone Research in Biomechanics* (eds Lowet G, Ruegsegger P, Weinans H, Meunier A), pp. 33–48. Tokyo: Ohmsha Ltd.

Hurwitz DE, Sumner DR, Andriacchi TP, Sugar DA (1998) Dynamic knee loads during gait predict proximal tibial bone distribution. *J Biomech* **31**:423–430.

Hutton WC, Elmer WA, Bryce LM, Kozlowska EE, Boden SD, Kozlowski M (2001) Do the intervertebral disc cells respond to different levels of hydrostatic pressure? *Clin Biomech* **16**, 728–734.

Ikenoue T, Trindade MCD, Lee MS, et al. (2003) Mechanoregulation of human articular chondrocyte aggrecan and type II collagen expression by intermittent hydrostatic pressure in vitro. *J Orthop Res* **21**, 110–116.

Kaplan PA, Gehl RH, Dussault RG, Anderson MW, Diduch DR (1999) Bone Contusions of the posterior lip of the medial tibial plateau (contrecoup injury) and associated internal derangements of the knee at MR imaging. *Radiology* **211**, 747–753.

Kippel JH, Dieppe PA, eds (1994) *Rheumatology*. St. Louis: Mosby-Year Book.

Laor T, Chun GFH, Dardzinski BJ, Bean JA, Witte DP (2002) Posterior distal femoral and proximal tibial metaphyseal stripes at MR imaging in children and young adults. *Radiology* **224**, 669–674.

Li G, Lopez O, Rubash H (2001) Variability of a three-dimensional finite element model constructed using magnetic resonance images of a knee for joint contact stress analysis. *J Biomech Eng* **123**, 341–346.

Lyyra T, Jurvelin J, Pitkänen P, Väätäinen U, Kiviranta I (1995) Indentation instrument for the measurement of cartilage stiffness under arthroscopic control. *Med Eng Phys* **17**, 395–399.

Mow VC, Proctor CS, Kelly MA (1989) Biomechanics of articular cartilage. In *Basic Biomechanics of the Musculoskeletal System* (eds Nordin M, Frankel VH), pp. 31–58. Philadelphia: Lee and Febiger.

Murray P, Drachman D (1969) The role of movement in the development of joints and related structures: the head and neck in chick embryos. *J Embryol Exp Morphol* **22**, 349–371.

Murray RC, Vedi S, Birch HL, Lakhani KH, Goodship AE (2001) Subchondral bone thickness, hardness and remodelling are influenced by short-term exercise in a site-specific manner. *J Orthop Res* **19**, 1035–1042.

Plochocki JH, Riscigno CJ, Garcia M (2006) Functional adaptation of the femoral head to voluntary exercise. *Anat Rec* **288**, 776–781.

Radin EL, Orr RB, Kelman JL, Paul IL, Rose RM (1982) Effect of prolonged walking on concrete on the knees of sheep. *J Biomech* **15**, 487–492.

Rohlf F (1998) *TpsDig version 1.23*. Stonybrook, NY: State University of New York at Stonybrook.

Saarakkala S, Korhonen RK, Laasanen MS, Töyräs J, Rieppo J, Jurvelin JS (2004) Mechano-acoustic determination of Young's modulus of articular cartilage. *Biorheology* **41**:167–179.

Shelburne KB, Torry MR, Pandy MG (2006) Contributions of muscles, ligaments, and the ground-reaction force to tibiofemoral joint loading during normal gait. *J Orthop Res* **24**:1983–1990.

Sironen RK, Karjalainen HM, Elo MA, et al. (2002) cDNA array reveals mechanosensitive genes in chondrocytic cells under hydrostatic pressure. *Biochim Biophys Acta* **1591**, 45–54.

Smith DE (1997) *Design optimization*. In *ASM Handbook, Vol. 20, Materials Selection and Design*. ASM International Publications, pp. 209–218.

Smith RL, Carter DR, Schurman DJ (2004) Pressure and shear differentially alter human articular chondrocyte metabolism: a review. *Clin Orthop Relat Res* **427** Suppl, S89–95.

Smith RL, Rusk SF, Ellison BE, et al. (1996) In vitro stimulation of articular chondrocyte mRNA and extracellular matrix synthesis by hydrostatic pressure. *J Orthop Res* **14**, 53–60.

Smith RL, Lin J, Trindade MC, et al. (2000) Time-dependent effects of intermittent hydrostatic pressure on articular chondrocyte type II collagen and aggrecan mRNA expression. *J Rehab Res Dev* **37**, 153–161.

Steinberg ME, Trueta J (1981) Effects of activity on bone growth and development in the rat. *Clin Orthop* **156**, 52–60.

Stone JJ, Yu H (1997) Computational contact analysis of joint congruency. *Biomed Sci Instrum* **34**, 368–373.

Takahashi K, Kubo T, Kobayashi K, et al. (1995) Hydrostatic pressure influences mRNA expression of transforming growth factor-beta 1 and heat shock protein 70 in chondrocyte-like cell line. *J Orthop Res* **13**, 495–502.

Thambyaha A, Pereiraa BP, Wyssb U (2005) Estimation of bone-on-bone contact forces in the tibiofemoral joint during walking. *Knee* **12**, 383–388.

Tissakht M, Ahmed AM (1995) Tensile stress-strain characteristics of the human meniscal material. *J Biomech* **28**, 411–422.

Toyoda T, Seedhom BB, Kirkham J, Bonass WA (2003) Upregulation of aggrecan and type II collagen mRNA expression in bovine chondrocytes by the application of hydrostatic pressure. *Biorheology* **40**, 79–85.

Urban JGP (1994) The chondrocyte: a cell under pressure. *Br J Rheum* **33**, 901–908.

van de Lest CH, Brama PA, van Weeren PR (2002) The influence of exercise on the composition of developing equine joints. *Biorheology* **39**, 183–191.

Vanderplaat G (2002a) *VisualDOC version 3.0*. Colorado Springs, CO: Vanderplaat Research and Development, Incorporated.

Vanderplaat G (2002b) *VisualScript version 3.0*. Colorado Springs, CO: Vanderplaat Research and Development, Incorporated.

Vaughan CL, Damioano DL, Abel MF (1997) Gait of normal children and those with cerebral palsy. In *Three-Dimensional Analysis of Locomotion* (eds Allard P, Cappozzo A, Lundberg A, Vaughan CL), pp. 335–361. Chichester: Wiley.

von Eisenhart-Rothe R, Eckstein F, Muller-Gerbl M, Landgraf J, Rock C, Putz R (1997) Direct comparison of contact areas, contact stress and subchondral mineralization in human hip joint specimens. *Anat Embryol* **195**, 279–288.

Wagner DR, Lindsey DP, Li KW, et al. (2008) Hydrostatic pressure enhances chondrogenic differentiation of human bone marrow

stromal cells in osteochondrogenic medium. *Ann Biomed Eng* **36**, 813–820.

Williams PL (1995) *Gray's Anatomy*, 38th edn. London: Churchill Livingstone.

Wilson W, van Burken C, van Donkelaar C, et al. (2005) Causes of mechanically induced collagen damage in articular cartilage. *J Orthop Res* **24**, 220–228.

Wong M, Carter DR (2003) Articular cartilage functional histo-

morphology and mechanobiology: A research perspective. *Bone* **33**, 1–13.

Wong M, Siegrist M, Goodwin K (2003) Cyclic tensile strain and cyclic hydrostatic pressure differentially regulate expression of hypertrophic markers in primary chondrocytes. *Bone* **33**, 685–693.

Wretenberg P, Ramsey DK, Nemeth G (2002) Tibiofemoral contact points relative to flexion angle measured with MRI. *Clin Biomech* **17**, 477–485.